

CFD-ANALYSIS OF 3D FLOW STRUCTURE AND ENDWALL HEAT TRANSFER IN A TRANSONIC TURBINE BLADE CASCADE: EFFECTS OF GRID REFINEMENT

Alexander M. Levchenya* and Evgueni M. Smirnov*

**Department of Aerodynamics, St. Petersburg State Polytechnic University
 Polytechnicheskaya 29, 195251 St. Petersburg, Russia
 E-mail: aero@phmf.spbstu.ru, web: <http://aero.spbstu.ru>*

Key words: heat transfer, numerical simulation, transonic turbine cascade, grid refinement

Abstract. Results of numerical simulation of three-dimensional turbulent flow and endwall heat transfer in a transonic turbine cascade are presented. Employing several turbulence models (k - ω model by Wilcox, Menter SST model, v^2 - f model by Durbin), an analysis of Computational Fluid Dynamics (CFD) predictability was done in comparison with measurements in a linear cascade at the NASA Glenn Research Center transonic turbine blade cascade facility. It has been concluded in particular that rather fine computational grids are needed to get grid-independent data on the endwall local heat transfer controlled by complex 3D structure of secondary flows. With CFD codes of second-order accuracy, one should use grids comprised of about or more than 2 millions cells (for each full blade passage) to get a definite conclusion on preference of one or another turbulence model for predictions of phenomena under consideration.

NOMENCLATURE

c_p	[$J/kg \cdot K$]	specific heat
C_x	[m]	blade axial chord
k	[m^2/s^2]	turbulence kinetic energy
M	[-]	Mach number
P	[Pa]	pressure
Pr	[-]	Prandtl number
q_w	[W/m^2]	wall heat flux
r	[-]	recovery factor
R	[$J/kg \cdot K$]	gas constant
Re	[-]	Reynolds number, $Re = \rho U_{in} C_x / \mu$
St	[-]	Stanton number
T	[K]	temperature
U	[m/s]	velocity magnitude
x	[m]	chordwise (axial) direction
y^+	[-]	normalized distance to a wall
γ	[-]	specific heat ratio

ε	[m^2/s^3]	turbulence dissipation rate
μ	[$kg/s \cdot m$]	dynamic viscosity
ω	[$1/s$]	specific turbulence dissipation rate
ρ	[kg/m^3]	density

Subscripts and Superscripts

aw	adiabatic wall temperature
ex	exit freestream value
in	inlet freestream value
is	isentropic value
p	computational point nearest to a solid wall
ref	reference value
w	wall
x	axial
'	total conditions

1. INTRODUCTION

It is well known that three-dimensional secondary flows in blade rows can dramatically affect performance of gas turbines. Consequently, there is a strong need for computational models/tools that would allow accurate predictions of the secondary flow effects both on the pressure losses and heat transfer.

Development of three-dimensional structures in turbine blade rows are controlled mostly by flow physics in the layer adjacent to the endwall. The main factors are the deceleration of the endwall boundary layer, when approaching the blade leading edge (LE), and the flow turn in the blade passage. The first factor action is typical also for a wing-body junction, so the experience on modeling of 3D flow structure and heat transfer in blade rows can be useful for external aerodynamics applications as well.

CFD-analysis is a powerful tool to obtain data on 3D turbulent flow structure and local heat transfer that are necessary to design a turbine stage. However, a systematic work aimed at CFD model validation and grid dependence evaluation has to be performed comparing computational results with benchmark-quality experimental data. It should be emphasized here, that among other data of practical interest the local heat transfer data are the most sensitive to peculiarities of secondary flows, and, consequently, to details of physical and computational modelling.

The NASA Glenn Research Center (GRC) linear transonic blade cascade of a large-scale¹⁻³ is a test case specially designed to provide a detailed high Mach number rotor blade flow and heat transfer data set to CFD code developers and users. A brief description of the experimental facility and available data are as follows. The transonic turbine blade linear cascade with a large turning angle consists of 11 passages. A highly three-dimensional flow field was obtained in the blade passage by allowing the endwall turbulent boundary layer to develop in a long inlet section upstream of the cascade. To define the cascade inlet flow conditions, aerodynamic probe measurements were made at a section located one axial chord upstream of the blade leading edge plane. For the endwall heat transfer measurements under conditions of approximately constant wall heat flux, power settings were ranged from 200 to 1200 Watts. The net surface heat flux rate used to determine the Stanton number was the heater power corrected for conduction losses and for radiative heat transfer. The steady-state liquid crystal technique was used for surface temperature measurements. Local endwall heat transfer measurements were performed at eight combinations of the inlet Reynolds number, Re , the isentropic exit Mach number, M_{ex} , and the freestream turbulence intensity. Additional details are given by Giel *et al*².

Previously, the experimental data set obtained in the NASA GRC was used by Garg and Ameri⁴ to examine capabilities of two-equation turbulence models for prediction of blade heat transfer. Kalitzin *et al*⁵ computed blade and endwall heat transfer using the Durbin four-equation v^2-f model and the Spalart-Allmaras (S-A) one-equation model. Goriatchev *et al*⁶ analyzed secondary flows and pressure losses using the S-A model. Ivanov *et al*⁷ used different versions of S-A, $k-\varepsilon$ and $k-\omega$ turbulence models with the same grids. All these studies were performed using Navier-Stokes codes of second-order accuracy with block-structured computational grids consisting of about 350,000 to 550,000 cells (for one half of the blade passage height, in compliance with the assumption of the time-averaged flow symmetry). Analysis of the computational data reported allows a conclusion that computations with grids of such a size produce grid-

independent data on wall pressure distribution and shock position, but the grid sensitivity of local heat transfer and pressure losses remains questionable.

The present contribution covers CFD results obtained for the NASA GRC transonic turbine cascade with the code SINF being under long-time development at the Department of Aerodynamics of the St.-Petersburg State Polytechnic University.

Among the data provided by Giel *et al*¹⁻³, the experimental case of $Re = 1.0 \times 10^6$ and $M_{ex} = 1.3$ is chosen for the present study. Computational data obtained with several low- Re turbulence models ($k-\omega$ model by Wilcox⁸, the SST version of the Menter model⁹, the “code-friendly” version of the v^2-f model by Durbin¹⁰) and several computational meshes are compared thoroughly with the endwall heat transfer measurement results.

2. PROBLEM DEFINITION

The geometry of the linear cascade is that available from the NASA GRC CD-ROM database arranged by Giel and Gaugler³. A fragment of the cascade is illustrated in the Figure 1, together with a slice of the computational domain.

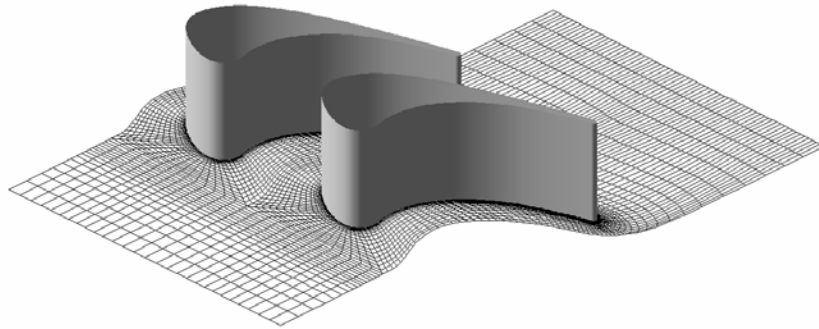


Figure 1. Blade passage and slice of the computational domain.

Axial chord, C_x , cm	12.7
Pitch, cm	13.0
Span, cm	15.24
True chord, cm	18.42
Design inlet flow angle, degrees	63.6
Total turning (at inlet flow angle), degrees	136
Prandtl number, Pr	0.72
Inlet Reynolds number, Re	1.0×10^6
Inlet Mach number, M_{in}	0.38
Exit Mach number, M_{ex}	1.32
Inlet boundary layer thickness, cm	3.2
Inlet turbulence intensity, %	0.25
Inlet turbulence length scale, cm	0.127

Table 1. Cascade dimensions and flow parameters

At the present computations, the fluid (air) is treated as a perfect gas with the specific heat ratio $\gamma=1.4$. The governing equations are the Reynolds-averaged Navier-Stokes equations and the energy equation written for the total enthalpy. A power-law is adopted to account for the dependency of viscosity on temperature, $\mu \sim T^{0.76}$.

In order to define proper boundary conditions at the 3D computational domain inlet section placed one axial chord upstream of the blade leading edge, the two-dimensional (2D) turbulent flow developing in a parallel-plate channel was computed first, assuming the adiabatic wall conditions. In the 2D flow computed separately for each of the turbulence model used, a section was chosen that corresponded to the boundary layer thickness of 3.2 cm. Flow field data at this section were used to define the total temperature, total pressure, velocity vector angle and turbulence parameters distributions over the inlet plane of the 3D blade cascade computational domain.

To get the isentropic Mach number required a proper value of static pressure was specified at the outlet boundary located one axial chord downstream of the blade trailing edge. At the solid surfaces of the cascade the no-slip condition was imposed. The constant temperature, T_w , of 350 K (that would correspond to power of 1560 Watts in the experimental prototype) was specified on the endwall, starting from the position of $0.3 \cdot C_x$ upstream of the blade leading edge. Remaining walls were treated as adiabatic. Periodic boundary conditions were used in the pitchwise direction. For computational purposes, only half of the real span was considered, with the symmetry boundary condition at mid-span.

3. COMPUTATIONAL ASPECTS

The 3D incompressible/compressible Navier-Stokes code SINF is based on the second-order finite-volume spatial discretization using the cell-centered variable arrangement and body-fitted block-structured grids. A general description of the code capabilities is given by Smirnov and Zajtsev¹¹. For transonic flow analysis, a high-order version of the Jameson's H-CUSP scheme¹² is implemented and tested¹³ in combination with a regularization technique removing the difficulties of compressible flow computations in low-Mach-number regions.

For the present analysis, a set of 3D non-uniform grids have been generated assuming the flow symmetry with respect to the passage middle plane. All the grids are of 3-block H-O-H structure (see Figure 1). Each mesh covers one half of the blade channel height, and was obtained by translation of a 2D grid along the spanwise direction. Grids of the best resolution have 45 nodes along this direction, clustered to the endwall. The distance from the first cell centre to the endwall was equal to $0.2 \times 10^{-4} C_x$ that produced the area-averaged y_p^+ -value of 0.8. As a result of special computations, it has been established that a further grid refinement with respect to the spanwise direction is not necessary.

Below the main attention is paid to the effects of grid refinement in the planes parallel to the endwall (in fact, a starting 2D grid refinement), especially in the leading edge region where 3D vortex structures arise. In order to characterize the grid quality in the LE region, we have introduced an averaged cell size, Δ^* , evaluated for the cells that are placed in the middle between the saddle (separation) point and the blade LE, except the boundary layer region adjacent to the blade. Note that this cell size is measured in the line of the LE, and the cell aspect ratio in this region did not exceed 2.0 for all the grids. Table 2 covers data for five of the grids, results for which are presented below. For the finest grid, the averaged cell size introduced is of 1% of the blade axial chord (or about

5% of the blade LE radius). Note also that the grid slice given in Figure 2 corresponds to grid B (every second grid line of the grid is omitted there for clarity).

Mesh	Number of cells	Δ^*/C_x	Refinement aspects
A	360,000	0.027	Initial grid
B	730,000	0.022	Add nodes for all the blocks, especially far away from the blade
C	750,000	0.022	Equalize cell aspect ratio in the free-stream flow region
D	760,000	0.017	Shift gridlines to the blade
E	1,200,000	0.01	Add nodes for all blocks, especially in the LE region

Table 2. Parameters of the grids used and refinement aspects.

To ensure a direct comparison of computational heat transfer results with the measurement data, local Stanton numbers were calculated using the same procedure as developed and justified by Giel *et al*². Remarkably that this procedure results in Stanton numbers that are practically independent of the surface heat flux rate varied in the experiments.

Under the operation conditions under consideration, the choice of temperature difference used as the driving potential and the choice of a reference temperature for gas thermophysical properties significantly affects the heat transfer coefficient. Having performed a comparison of various definitions, Giel *et al*² suggested to define the Stanton number as follows

$$St = \frac{q_w}{\rho_{\text{ref}} U_{\text{in}} c_p (T_w - T_{\text{aw}})}, \quad (1)$$

where the local adiabatic wall temperature, T_{aw} , is defined as

$$\frac{T_{\text{aw}}}{T_{\text{in}}} = r + \frac{1-r}{1 + 0.5(\gamma-1)M_{\text{is}}^2}, \quad (2)$$

In expression (2) the local isentropic Mach number, M_{is} , is determined from the wall static pressure, and the recovery factor, r , is evaluated as $r = Pr^{1/3}$. The density, ρ_{ref} , included in (1), unlike the value used for the Reynolds number is not the actual physical density. It is defined as

$$\rho_{\text{ref}} = P_{\text{in}}' / (RT_{\text{ref}}). \quad (3)$$

The air reference temperature, T_{ref} , used also for evaluation of the air molecular viscosity and heat conductivity is calculated as

$$T_{\text{ref}} = T_{\text{is}} + 0.5(T_w - T_{\text{is}}) + 0.22(T_{\text{aw}} - T_{\text{is}}). \quad (4)$$

The isentropic temperature, T_{is} , is evaluated using the local isentropic Mach number and the free-stream total temperature.

4. RESULTS AND DISCUSSION

Flow field computed is illustrated in Figures 2 and 3. Here, as an example, results obtained with grid B and the SST version of the Menter model (MSST) are given. It should be emphasized, however, that for the Mach number field and the static pressure

distribution over the blade all other combinations of grids A to E and the turbulence models (introduced above) produced practically identical results, if compared for the measurement planes indicated in Figure 3.

Figure 2 shows mid-span Mach number contours. Figure 3 presents blade pressure loading distributions at 50%, 25%, 10%, 5% and 2.5% span. The distributions computed are in an excellent agreement with the NASA GRC experimental data. The strong affection of the spanwise location on the static pressure distribution over the suction surface is well reproduced in the CFD-analysis. Near the trailing edge the computations predicts an increase in pressure on the suction side that is due to the flow overexpansion and viscous-inviscid interaction phenomena in the trailing edge region (see Figure 2).

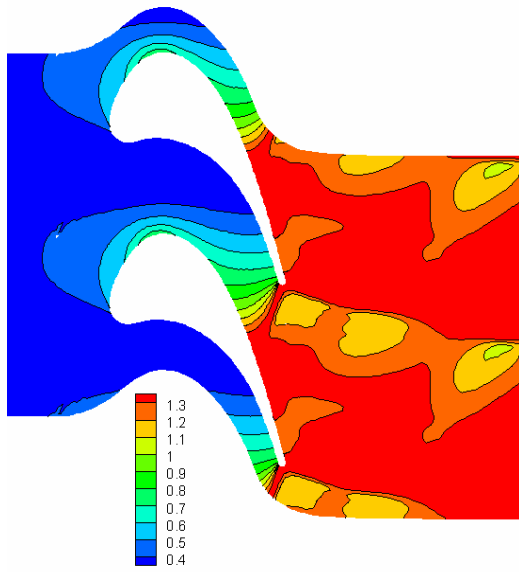


Figure 2. Computed mid-span Mach number distribution.

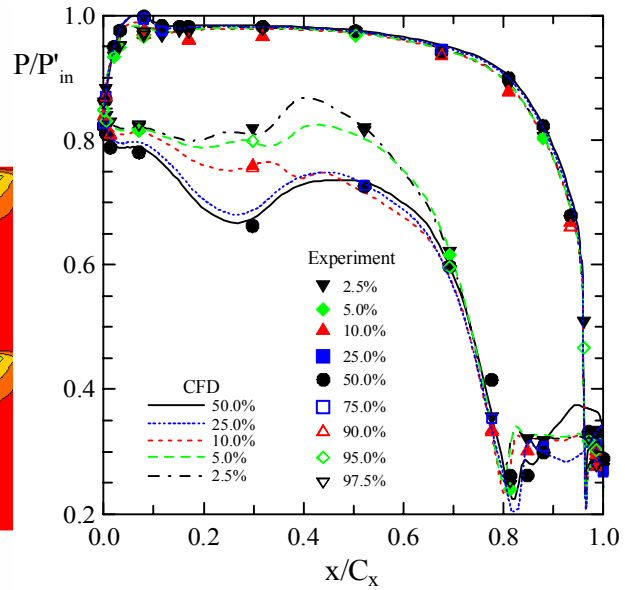


Figure 3. Comparison of computed and measured static pressure distributions over the blade surface for various span positions.

In contrast to the blade surface pressure distribution, computational results for local endwall heat transfer are very sensitive both to the turbulence model and the grid quality.

Figure 4 presents Stanton number distributions over the endwall computed with three turbulence models in comparison with the measurement data. These distributions were obtained using grid B. Generally one can conclude that all the models capture the main trends in formation of the local heat transfer pattern under action of 3D vortex structure developing in the blade passage. However, there are pronounced distinctions in the blade LE region where spots of enhanced heat transfer are observed. In particular, the $k-\omega$ model predicts a zone of the highest Stanton numbers that adjoins directly the leading edge, but the latter is in contradiction with the measurements. Both the MSST model and the v^2-f model predict crescent zones of extreme heat transfer placed slightly upstream of the blade LE. Such a crescent zone is seen in the experimental Stanton number distribution as well. At that, the v^2-f model gives a Stanton number distribution that is much more non-uniform as compared with the measurement data. All the models did not predict a spot of enhanced heat transfer observed in the experiments at the blade

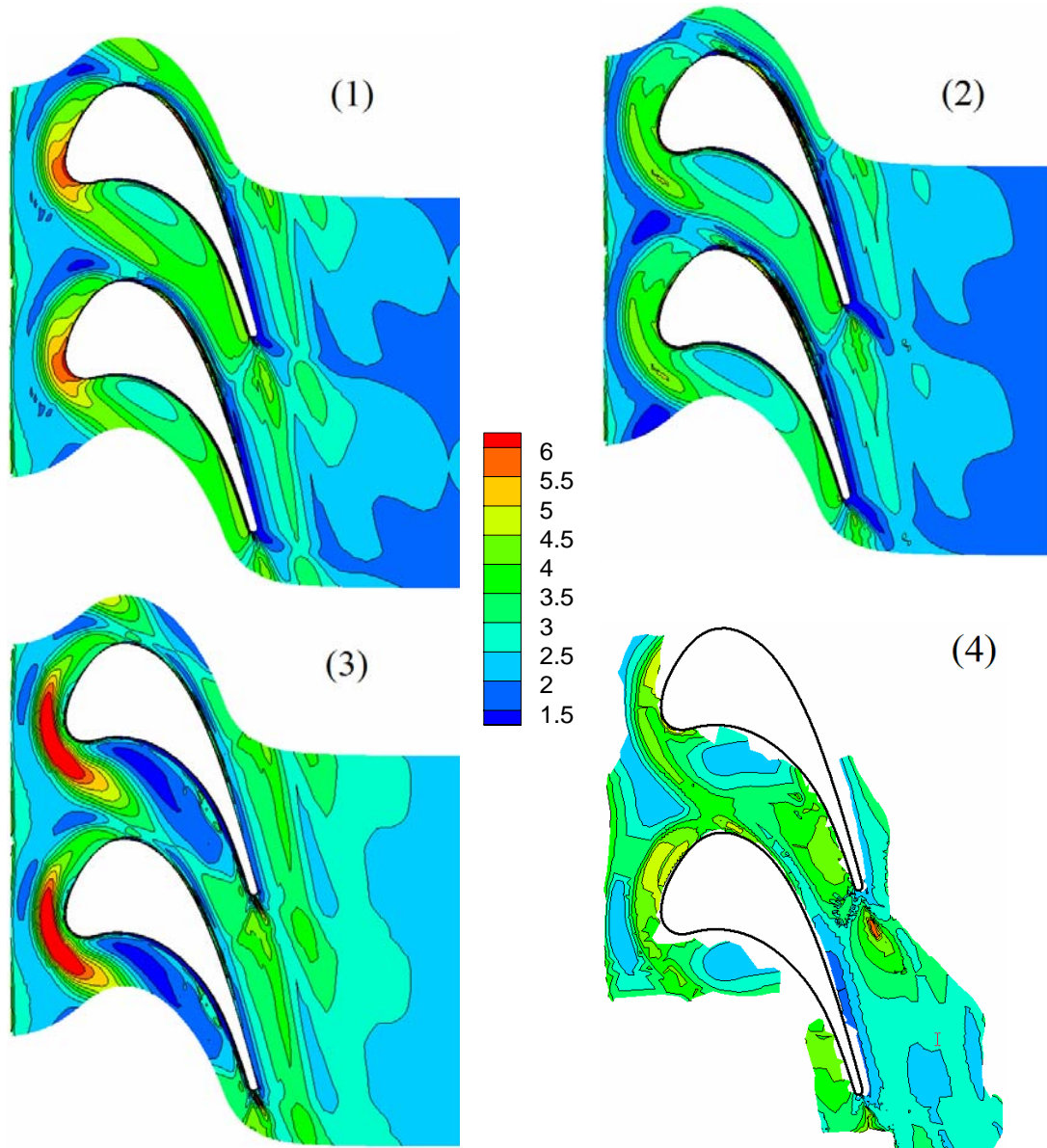


Figure 4. Endwall Stanton number ($\times 10^3$) distributions computed with grid B in comparison with the measurement data: (1) $k-\omega$ turbulence model, (2) MSST, (3) v^2-f , (4) experiment.

suction side not far from the leading edge. As a whole, the MSST model has prediction superiority among the turbulence models examined.

Now we concentrate at analysis of grid-sensitivity of local endwall heat transfer. This analysis is performed for the $k-\omega$ and the MSST turbulence models taking into account that currently they are rather popular in predictions of wall-bounded flows.

Our computations have shown that the $k-\omega$ model prediction results are considerably less sensitive to grid refinement as compared with the MSST model. With the $k-\omega$ model, grids B to E produced practically identical results. Small distinctions in the endwall Stanton number distributions are observed only when comparing results obtained using the initial grid (grid A) with those of one of the finer grids. It is illustrated in Figure 5. Below we discuss the reasons of relatively weak grid-sensitivity of the $k-\omega$ model results for the problem under consideration.

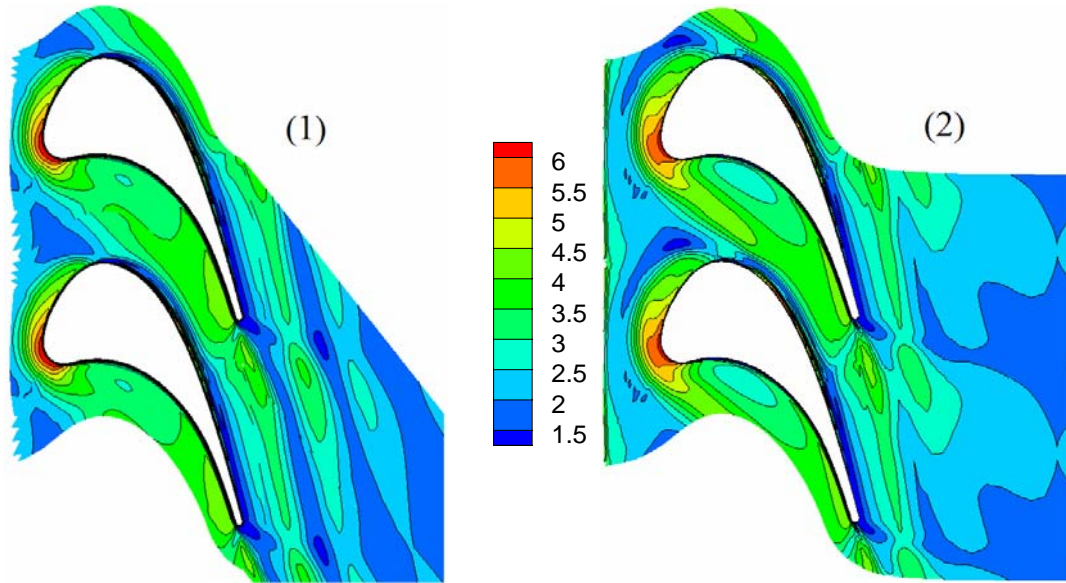


Figure 5. Endwall Stanton number ($\times 10^3$) distributions computed with the $k-\omega$ turbulence model: (1) grid A, (2) grid B.

Figure 6 illustrates the effect of grid refinement on the endwall Stanton number distributions computed with the MSST turbulence model (in order to sharpen the effect, in this figure the upper limit of the color legend is decreased as compared with Figure 4). The simulation results are very sensitive to the grid quality in the region placed upstream of the blade LE, where horseshoe vortex structures arise. Grid refinement results in formation of two crescent zones of extreme heat transfer (see the St maps for grid D and E), whereas only one such a zone was observed when using coarser grids (see the St map for grid C, as well as Figure 4-2). Remarkably that even for grids C and D, comprised of about same numbers of cells, there is a considerable difference between the results for zones of high Stanton numbers. Grid E produces the most detailed pattern of the Stanton number distribution.

It should be recognized however that the grid refinement has not resulted in a considerably better agreement between the computational and measurement data. In particular, as in the coarser grid case, the finest grid computations do not predict the high-St spot observed in the experiments at the blade suction side not far from the leading edge. As well, the St values are underestimated at the pressure side near the blade trailing edge.

Let's discuss now the reasons of considerable distinctions between the endwall heat transfer prediction results obtained for the blade LE region with the $k-\omega$ turbulence model and the MSST model. A detailed analysis of the flow structure in the endwall boundary layer just upstream of the blade LE has shown that the $k-\omega$ model produces a much simpler flow topology than the MSST model, provided fine grids are used in both the cases. For the MSST model case, Figure 7 presents a pattern of limiting streamlines on the endwall computed with grid E. One can see trails of a number of well-resolved vortex structure determining the endwall heat transfer peculiarities in the blade cascade under consideration. The section A-A marked in the blade LE region was used for visualization (see Figure 8) of the near-endwall flow topology in the normal plane. With

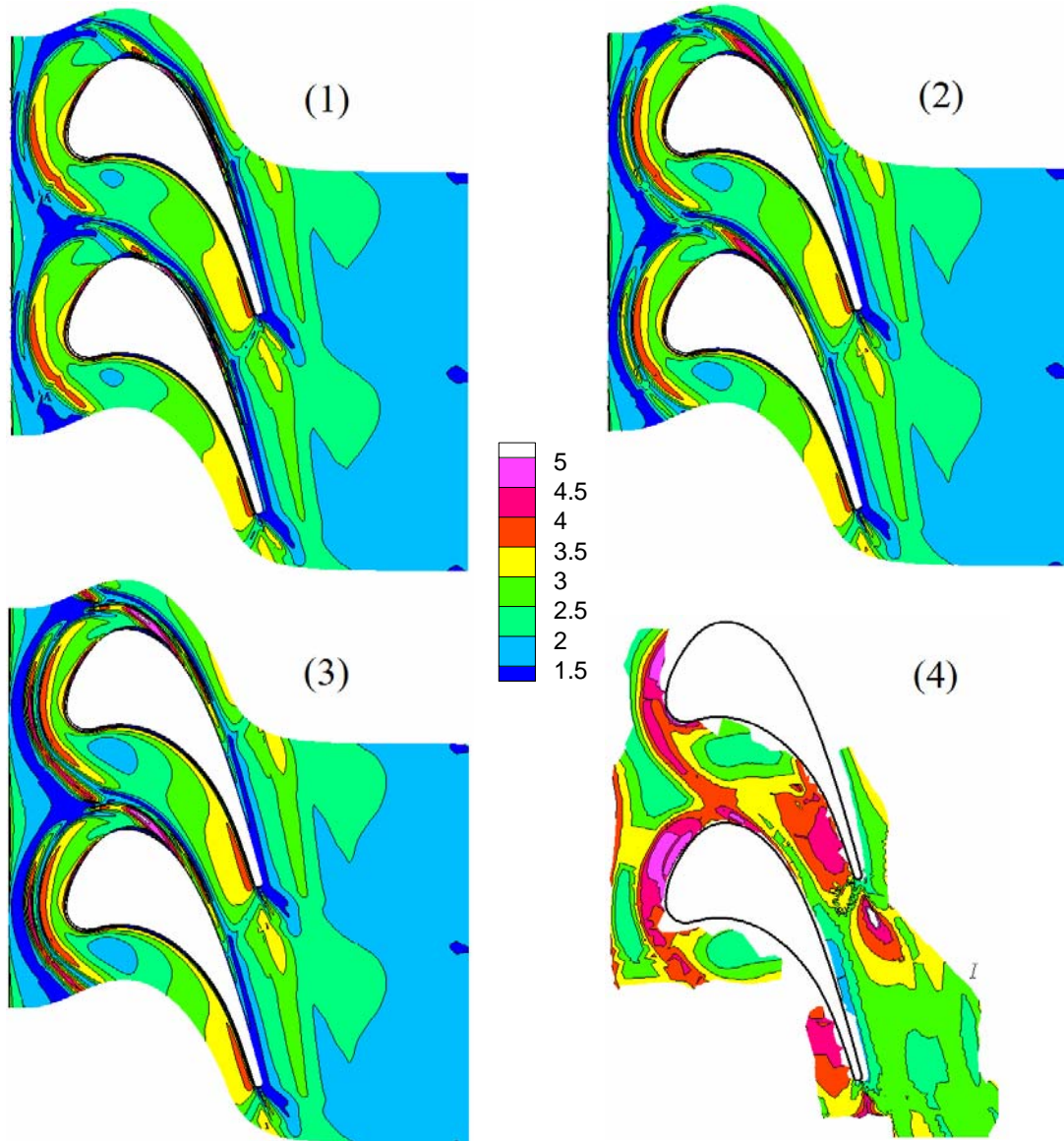


Figure 6. Effect of grid refinement on the endwall Stanton number ($\times 10^3$) prediction with the MSST turbulence model: (1) grid C, (2) grid D, (3) grid E, (4) experiment.

a fine grid, the MSST model predicts a complicated vortex structure: with the main horseshoe vortex, a counter rotating secondary vortex located closer to the endwall and a tertiary vortex. Application of a similar visualization technique to the flow field computed with the $k-\omega$ model has shown that a structure with one horseshoe vortex is predicted, and intensity of this vortex is reduced as compared with the main vortex predicted by the MSST model.

Previously, such a kind of distinctions was reported by Levchenya *et al*¹⁴ when analysing numerical simulation results for the 3D turbulent flow and endwall heat transfer in a cascade of thick vanes. In that contribution it was reported also that, at least in the region of the horseshoe vortex formation, the $k-\omega$ model produces a higher level of the eddy viscosity than the MSST model, and it is a main reason of distinctions in the flow topology upstream of the blade leading edge.

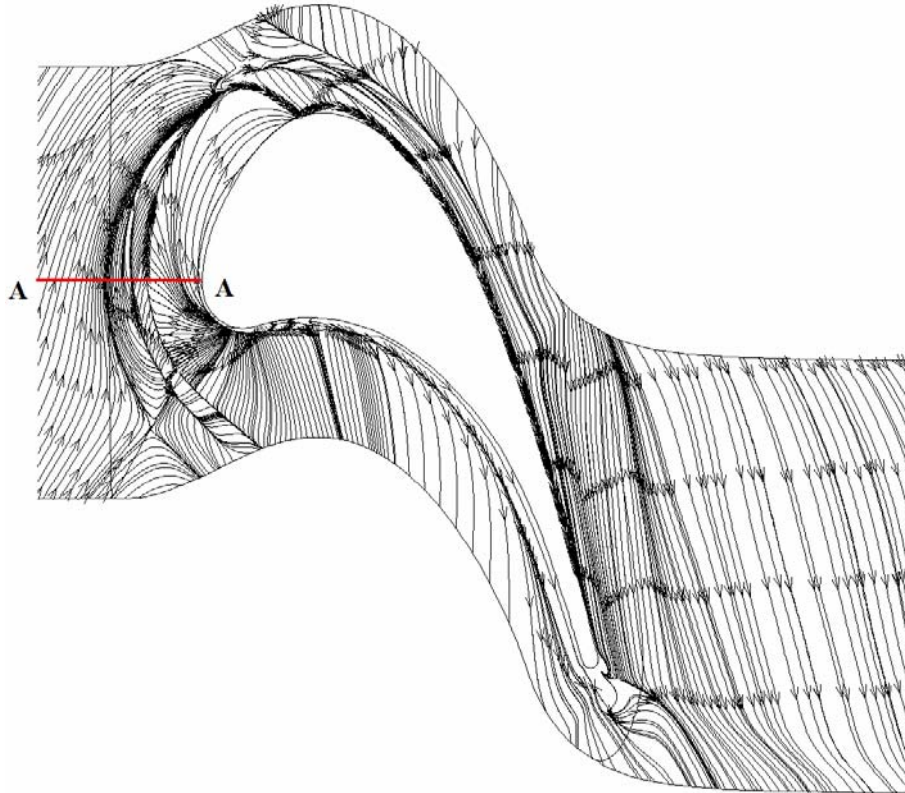


Figure 7. Endwall streakline visualization.

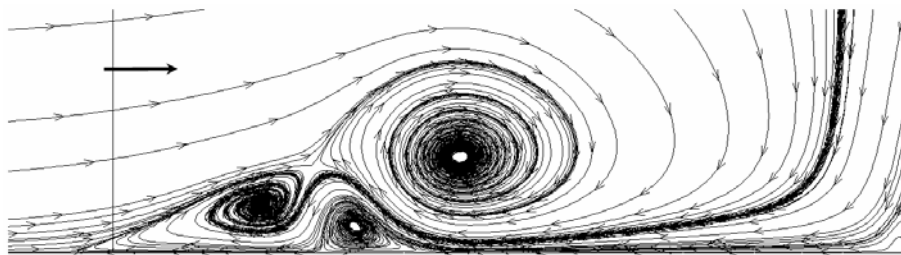


Figure 8. Streamline topologies in plane A-A, as defined in Figure 7

5. SUMMARY

With an in-house finite-volume Navier-Stokes code of second-order accuracy, effects of computational grid refinement have been investigated for the problem of 3D turbulent flow and endwall heat transfer in a linear transonic turbine cascade with a large turning angle, and under low freestream turbulence conditions. Three turbulence models were used at the computations ($k-\omega$ model by Wilcox, Menter SST model, v^2-f model by Durbin). The main attention for the grid-sensitivity aspects was paid to the cases of the $k-\omega$ and the MSST since currently they are rather popular in predictions of wall-bounded flows.

It has been established that the MSST model prediction results are considerably more sensitive to grid refinement as compared with the $k-\omega$ model, especially for the flow and heat transfer region placed upstream of the blade leading edge, where horseshoe vortex structures arise. A less grid-sensitivity of the $k-\omega$ model is due to the fact that generally it produces a higher level of the eddy viscosity, and it results in prediction of a simplified flow topology as compared with the MSST model.

As a whole, one can conclude that rather fine computational grids are needed to get grid-independent data on the endwall local heat transfer controlled by complex 3D structure of secondary flows. With CFD codes of second-order accuracy, one should use grids comprised of about or more than 2 millions cells (for each full blade passage) to get a definite conclusion on capabilities of one or another turbulence model for predictions of phenomena under consideration.

ACKNOWLEDGMENTS

The authors wish to thank Dr. Paul W. Giel, NASA Glenn Research Center, for the help in getting the cascade geometry and measurement data. The work was partially supported by the Russian Foundation of Basic Research, Grant No. 06-08-01334.

REFERENCES

- [1] Giel, P.W., Thurman, D.R., Lopez, I., Boyle, R.J., Van Fossen, G.J., Jett, T.A., Camperchioli, W.P., and La, H., "Three-dimensional flow field measurements in a transonic turbine cascade," ASME Paper 96-GT-113 (1996).
- [2] Giel, P.W., Thurman, D.R., Van Fossen, G.J., Hippensteele, S.A, and Boyle, R.J., "Endwall heat transfer measurements in a transonic turbine cascade," ASME Paper 96-GT-180 (1996)
- [3] Giel, P.W., and Gaugler, R.E., "NASA Blade 1. Endwall heat transfer data. Version 1," NASA-Glenn Research Center, Turbine Branch, CD ROM (2001).
- [4] Garg, V.K., and Ameri, A.A., "Two-equation turbulence models for prediction of heat transfer on a transonic turbine blade," *Int. J. Heat and Fluid Flow*, Vol. 22, 593-602 (2001).
- [5] Kalitzin, G., and Iaccarino, G., "Computation of heat transfer in a linear turbine cascade", *Center for Turbulence Research Annual Research Briefs*, 277-288 (1999).
- [6] Goriatchev, V., Ivanov, N., Ris, V., and Smirnov, E., "CFD-analysis of secondary flows and pressure losses in a NASA transonic turbine cascade", In: «Modelling Fluid Flow. The State of the Art», J. Vad, T. Lajos & R. Schilling editors, Springer-Verlag Berlin Heidelberg, 2004. 311-321 (2004).
- [7] Ivanov, N., Ris, V., Smirnov, E., Telnov, D., "Numerical simulation of endwall heat transfer in a transonic turbine cascade", *Proceedings of the 12th International Conference on Fluid Flow Technologies*, Budapest, 1121-1128 (2003).
- [8] Wilcox, D.C., "A two-equation turbulence model for wall-bounded and free-shear flows", *AIAA Paper 93-2905* (1993).
- [9] Menter, F.R., "Two equation eddy-viscosity turbulence models for engineering applications", *AIAA Journal*, Vol. 32, 1598-1605 (1994).
- [10] Lien, F.S., Durbin, P.A., and Parneix, S., "Non-linear v_2 -f modeling with application to aerodynamic flows", *Proc. 8-th Symposium on Turbulent Shear Flows*, Grenoble, France, 8-10 Sep., Vol.1, Sec. 6, 19-24 (1997).

- [11] Smirnov, E.M., and Zajtsev D.K., “The finite-volume method in application to complex-geometry fluid dynamics and heat transfer problems”, Scientific-Technical Bulletin of the St.-Petersburg State Technical University, No 2(36), 70-81 (in Russian, 2004).
- [12] Jameson, A., “Positive schemes and shock modelling for compressible flows”, Int. J. Num. Meth. Fluids, Vol. 20, 743-776 (1995).
- [13] Nikolaev, M.A., “Combination of the CUSP scheme with the compressibility scaling method for transonic flow calculations in domains of complex geometry,” In: Phys. Principles of Exp. and Math. Simulation of Heat and Mass Transfer and Gas Dynamics in Power Plants. Proc. 13th Int. Leontiev’s School-Seminar, MPEI Publishers, Moscow, Russia, Vol.1, 108-111 (in Russian, 2001).
- [14] Levchenya, A.M., Ris, V.V., and Smirnov, E.M., “Testing of turbulence models as applied to calculations of 3D flow and endwall heat transfer in cascades of thick vane blades”, Proc. 4th Russian National Heat Transfer Conf., MPEI Publishers, Moscow, Russia, Vol.2, 167-170 (in Russian, 2006).